INTERNATIONAL JOURNAL FOR NUMERICAL METHODS IN FLUIDS
Int. J. Numer. Meth. Fluids 2007; **53**:333–351
Published online 19 June 2006 in Wiley InterScience (www.interscience.wiley.com). DOI: 10.1002/fld.1282

Lattice Boltzmann-based single-phase method for free surface tracking of droplet motions

Xiu Qing Xing, David Lee Butler*,† and Chun Yang

School of Mechanical and Aerospace Engineering, Nanyang Technological University, 50 Nanyang Avenue, Singapore 639798, Singapore

SUMMARY

A 2D single-phase free surface tracking model, based on the lattice Boltzmann method (LBM) is developed for simulating droplet motion. In contrast to the conventional multi-phase models, it is not necessary to simulate the motion of the gas phase using this 2D single-phase algorithm, and thus improves the computational efficiency without sacrificing the underlying physics. A method for special treatment of the relevant boundary conditions in the single-phase algorithm is proposed and also validated. Numerical simulations are carried out for the motion of a free falling droplet with or without considering gravity and droplet spreading under gravity. The simulations of the LBM are found to be consistent with the results obtained from commercial computational fluid dynamics (CFD) software Fluent. Copyright © 2006 John Wiley & Sons, Ltd.

Received 1 February 2006; Revised 20 April 2006; Accepted 23 April 2006

KEY WORDS: lattice Boltzmann method; free surface tracking; boundary conditions

1. INTRODUCTION

Lattice Boltzmann method (LBM) started to attract an attention in the CFD field only recently and it has been particularly successful in simulations of fluid flow applications involving complicated boundaries and complex fluids. Examples can be found for the Rayleigh–Taylor instability between two fluids in Reference [1], flows with substantial shock waves in Reference [2], processes with chemical reaction in References [3, 4], turbulent combustion in Reference [5], particles suspended in fluids performed by Ladd [6–8], Ladd and Verberg [9], Behrand [10], Aidun and Lu [11], and Masselot and Chopard [12], dynamics of colloidal systems in References [13–16], flow dynamics

*Correspondence to: David Lee Butler, School of Mechanical and Aerospace Engineering, Nanyang Technological University, 50 Nanyang Avenue, Singapore 639798, Singapore.
†E-mail: mdlbutler@ntu.edu.sg

Contract/grant sponsor: Agency for Science, Technology and Research; contract/grant number: 0421010018

in porous media in References [17–19], polymer solutions in Reference [20], mass/heat transfer flows in References [21–25].

The simulation of flows with free surfaces is important in a variety of technical applications such as flow through porous media, boiling dynamics and etching processes. Difficulties associated with the simulation of these types of problems lie in modelling the interface dynamics and dealing with the complex boundaries, as well as chemical reactions between fluid and solid surfaces. The objective of this paper is therefore to develop an LBM-based single-phase model for simulation of flows with free surfaces.

In the literature, several LBM models to simulate the interfacial dynamics have been successfully developed in the past decade. A brief review is provided here.

(a) *Colour model*. The colour model proposed by Gunstensen and Rothman [26] for simulating immiscible binary fluids is based on Lattice Gas model of Rothman and Keller [27]. The distribution function f_i on link i is assumed to be the sum of the two colour distribution functions denoted by superscript r (red) and b (blue), $f_i = f_i^{\mathrm{r}} + f_i^{\mathrm{b}}$. The distribution function is collided according to the lattice Boltzmann equation to give the new distribution function f'. The new distribution function f' is then perturbed to an alternative value f'' according to the colour gradient $\mathbf{g}(\mathbf{x})$ and the angle between the colour gradient vector and the coordinate axes. $\mathbf{g}(\mathbf{x})$ is defined by

$$\mathbf{g}(\mathbf{x}) = \sum_i \sum_j \mathbf{e}_j [f_j^{\mathrm{r}}(\mathbf{x} + \mathbf{e}_i) - f_i^{\mathrm{b}}(\mathbf{x} + \mathbf{e}_i)] \tag{1}$$

where $\mathbf{e}$ is the velocity vector. New distribution functions for the red and blue fluid can be then obtained by solving a maximization problem subjected to the conservation of mass and conservation of colour.

Grunau *et al*. [28] extended this model to allow for a variation of density and viscosity. D'Ortona *et al*. [29] studied the surface tension and wetting properties by modifying this model and obtained good agreement with theory. Nie *et al*. [30] extended the model of Gunstensen and Rothman [26] and Grunau *et al*. [28] for studying the two-dimensional Rayleigh–Taylor instability, and good agreement with experimental and analytical studies was obtained.

(b) *Method of Shan and Chen*. Shan and Chen [31, 32] and Shan and Doolen [33] considered a fluid with S different components on a regular lattice. In order to include the surface tension, they modified the LBM equation to:

$$f_i^k(\mathbf{x} + \mathbf{e}_i, t + 1) = f_i^k(\mathbf{x}, t) - \frac{f_i^k - f_i^{k(\mathrm{eq})}}{\tau} + \mathbf{e}_i \cdot \mathbf{F}^k(\mathbf{x}) \tag{2}$$

Here the force on the kth phase owing to a pairwise interaction between different phases is given by $\mathbf{F}^k(\mathbf{x})$. $f_i(\mathbf{x}, t)$ is the particle velocity distribution function at position $\mathbf{x}$ and time t along the ith direction. τ is the relaxation time. It should be noted that the collision operator $\mathbf{e}_i \cdot \mathbf{F}^k(\mathbf{x})$ in this model does not satisfy local momentum conservation.

(c) *Free energy approach*. This model was proposed by Orlandini *et al*. [34] and Swift *et al*. [35, 36] for simulating binary fluids and liquid–gas fluids. In this model, the total density ρ and the density difference $\Delta\rho$ are considered instead of using the densities of the two separate fluids ρ_{r} and ρ_{b} as the colour model does. Two distribution functions f_i and Δ_i are

DOI: 10.1002/fld

then used to describe the population of ρ and $\Delta\rho$, respectively, on each of the i links. Both distribution functions are governed by the single relaxation time Boltzmann equation.

This model was used by Buick [37] and Buick *et al.* [38] to simulate interfacial waves between two fluids, Xu *et al.* [39] to simulate phase-separating binary fluids under an oscillatory shear, Dupuis and Yeomans [40, 41] to simulate droplets on superhydrophobic surfaces and chemical heterogeneous surfaces, Palmer and Rector [42] to simulate thermal two-phase flow, Takada *et al.* [43] to simulate bubble motion under gravity, and Zhang *et al.* [44] to simulate droplet movements and continuous flows in rough and hydrophobic microchannels. The drawback of the free energy model is that the liquid–gas model is not Galilean invariant.

(d) *Model of He et al.* He *et al.* [1, 23] proposed a lattice Boltzmann scheme for simulation of multiphase flows with nearly incompressible limits. In their model, the interfacial dynamics such as phase segregation and surface tension are modelled by incorporating molecular interactions. An index function is introduced to track interfaces between different phases. Application to Rayleigh–Taylor instability yielded satisfactory results without any artificial reconstruction steps. This model was also validated in Reference [45] to simulate the spreading of a liquid droplet on a heterogeneous surface.

(e) *Free surface models*. Besides the multiphase and multi-component models, there are a couple of free surface models developed for simulating the moving interface between immiscible gas and liquid fluids. The distinctive feature of the free surface models is that the stream and collision processes are carried out only in the lattice units or cells that are occupied partially or fully by the fluid. This significantly reduces the computational complexity of the methods. It allows a relatively simple treatment of the free surface boundary conditions with high computational efficiency but without sacrificing the underlying physics.

One free surface model proposed by Ginzburg and Steiner [46] assumes that the collision only occurs on the 'active' cells which are fully or partially filled with fluid. The mass fraction of a cell filled with fluid, which is between zero and one, is an additional variable. A 're-colouring operator' similar to that in the model of Gunstensen and Rothman [26] determines the redistribution of fluid mass carried by each particle population. The macroscopic variables propagate together with the particle distribution functions in the stream step. The unknown particle distribution functions at the front of free surfaces, which cannot be obtained by the usual LBM, are constructed by using the first-order Chapman–Enskog expansion of the distribution functions. The drawback of this algorithm is that the construction steps are quite complicated.

Another free surface algorithm for gas–liquid interface simulations was proposed by Thürey [47], Thürey and Rüde [48], Thürey *et al.* [49], and Körner *et al.* [50]. It was originally developed for the simulation of metal foams to optimize and enhance the production process. The main character of this method is that the gas phase has negligible influence on the liquid phase and thus is not simulated as a fluid. Then the reconstruction step becomes quite easy. Due to its simplicity, high computational efficiency and low memory request, we will use this model as our basic model.

This paper is organized as follows: the single-phase free surface model is introduced first. Then, a method is proposed for special treatment of the relevant boundary conditions and incorporating external forces like gravity. After that the validation is carried out by simulating a free falling droplet with or without gravity and droplet spreading on a wall surface. The paper will conclude with a discussion on the results obtained.

DOI: 10.1002/fld

2. ALGORITHM

2.1. General LBM algorithm D2Q9 BGK model

Standard lattice topology classification D2Q9 BGK model is given by [51]:

$$f_i(\mathbf{x}+\mathbf{e}_i, t+\Delta t) = f_i(\mathbf{x}, t) - \frac{f_i - f_i^{\mathrm{eq}}}{\tau} \tag{3}$$

where superscript eq denotes the equilibrium state. Velocity vectors $\mathbf{e} = (0,0), (1,0), (0,1), (-1,0), (0,-1), (1,1), (-1,1), (-1,-1), (1,-1)$ in lattice units are shown in Figure 1. The density and velocity can be calculated by summation of all the distribution functions for one cell:

$$\rho = \sum_{i=0}^{8} f_i, \quad \rho\mathbf{u} = \sum_{i=0}^{8} \mathbf{e}_i f_i \tag{4}$$

The equilibrium distribution function can be chosen as

$$f_i^{\mathrm{eq}} = w_i \left[\rho + \frac{\mathbf{e}_i \cdot \mathbf{u}}{c^2} + \frac{(\mathbf{e}_i \cdot \mathbf{u})^2}{2c^4} - \frac{\mathbf{u}^2}{2c^2} \right] \tag{5}$$

where $c^2 = \frac{1}{3}$, and $w_i = 4/9$ for $i = 0$, $w_i = 1/9$ for $i = 1, 2, 3, 4$, and $w_i = 1/36$ for $i = 5, 6, 7, 8$.

2.2. Single-phase free surface model

Unlike other multi-phase models in which separate particle distribution functions are used for each phase, the single-phase free surface algorithm does not include the gas phase in the simulation. The different phases only use a same lattice, and are distinguished by flags for each lattice cell in the grid. Each cell might have three types: filled (fluid) cell, interface cell or empty (gas) cell. The

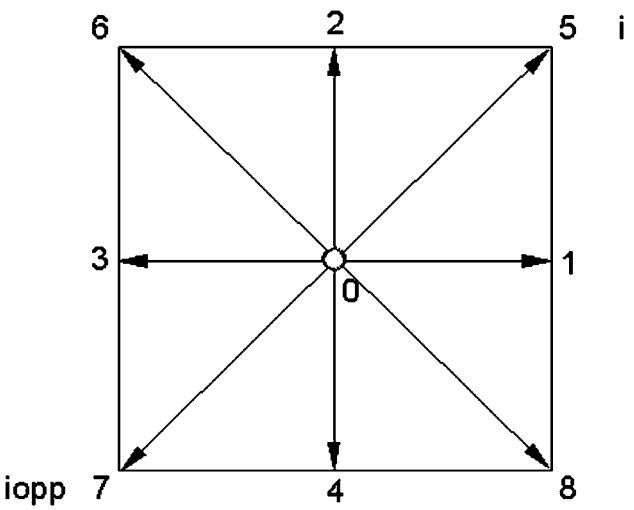

Figure 1. Topology of a D2Q9 lattice.

DOI: 10.1002/fld

complicated part of this model lies in how to deal with the interface cells, which form a closed layer between the fluid and empty cells.

In this model, tracking the free surface consists of three steps: the computation of the interface movement, the reconstruction of the unknown distribution functions at the fluid interface streamed from empty cells into interface cells, and the re-initialization of the cell types. The basic idea of free surface tracking is similar to Threy's model but the wall boundary conditions and gravity are treated using a method proposed in this study. The overview of the algorithm by Thürey *et al*. [49] is provided below.

2.2.1. Interface movement. The movement of the fluid interface is tracked by calculating the mass m contained in each cell and the fluid fraction ε which equals to the mass divided by the density ρ, i.e. $\varepsilon = m/\rho$. The flux between two cells can be directly computed from the values that are streamed between two adjacent cells. For an interface cell at $\mathbf{x}$ and a fluid cell at $(\mathbf{x}+\mathbf{e}_i)$, the mass flux is expressed as

$$\Delta m_i(\mathbf{x}, t+\Delta t) = f_{i_{\text{opp}}}(\mathbf{x}+\mathbf{e}_i, t) - f_i(\mathbf{x}, t) \tag{6}$$

Here, subscript i_{opp} denotes the value from the reverse direction of a value with subscript i. Thus f_i and $f_{i_{\text{opp}}}$ are the opposite distribution functions with reverse velocity vectors $e_i = -e_{i_{\text{opp}}}$. For instance, if $i=5$, then the $i_{\text{opp}}=7$, as shown in Figure 1. The first distribution function in Equation (6), $f_{i_{\text{opp}}}(\mathbf{x}+\mathbf{e}_i, t)$ is the amount of fluid entering this cell in the current time step, and the second one, $f_i(\mathbf{x}, t)$ is the amount leaving the cell. The mass exchange for two interface cells has to take into account the area of the fluid interface between the two cells. This is approximated by averaging the fluid fraction values of the two cells. Hence, it is calculated by

$$\Delta m_i(\mathbf{x}, t+\Delta t) = [f_{i_{\text{opp}}}(\mathbf{x}+\mathbf{e}_i, t) - f_i(\mathbf{x}, t)]\frac{\varepsilon(\mathbf{x}+\mathbf{e}_i, t) + \varepsilon(\mathbf{x}, t)}{2} \tag{7}$$

Therefore, for interface cells the mass change values for all directions are added to the current mass, resulting in the mass for the next time step:

$$m(\mathbf{x}, t+\Delta t) = m(\mathbf{x}, t) + \sum_{i=1}^{8} m_i(\mathbf{x}, t+\Delta t) \tag{8}$$

As for filled (fluid) cells, no mass exchange computations are necessary. Their fluid fractions (ε) are always equal to one and thus their mass equals their current density.

2.2.2. Reconstruction. In this algorithm, the empty cells are never accessed. However, the interface cells always have empty neighbours. Thus during the streaming steps, only the distribution functions from filled or interface cells can be streamed normally. Those coming out of empty cells and entering into interface cells need to be reconstructed since they are unknown.

If there is an interface cell at $\mathbf{x}$, and an empty cell at $(\mathbf{x}+\mathbf{e}_i)$, the distribution function entering into the interface and out of the empty cell can be expressed as

$$f'_{i_{\text{opp}}}(\mathbf{x}, t+\Delta t) = f_i^{\text{eq}}(\rho_A, \mathbf{u}) + f_{i_{\text{opp}}}^{\text{eq}}(\rho_A, \mathbf{u}) - f_i(\mathbf{x}, t) \tag{9}$$

where $\mathbf{u}$ is the velocity of the cell at position $\mathbf{x}$ and time t according to standard LBM notations, while $\rho_A = 1$ by assuming the gas has a default lattice density without considering the surface tension. This can be understood in the following way: Assuming that the effect of the gas phase on

DOI: 10.1002/fld

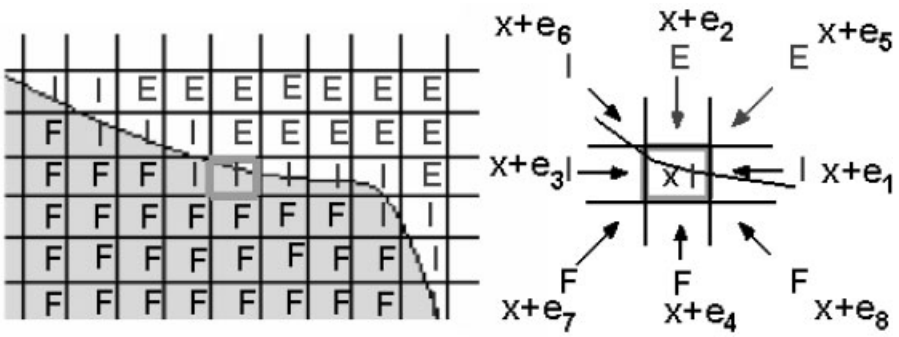

Figure 2. Reconstruct distribution functions from empty cells.

fluid motion can be ignored, as the gas reaches equilibrium state much faster than the fluid does due to low density. At the interface the gas moves the same way as the fluid does, so the distribution functions that will stream from a gas (empty) cell into an interface cell can be determined by the two opposite equilibrium distribution functions of the gas and the motion of the fluid represented by $f_i(\mathbf{x}, t)$. For instance, as shown in Figure 2, the cell at $\mathbf{x}$ is an interface cell, marked with 'I', with its neighbour empty cells at $\mathbf{x}+\mathbf{e}_2$ and $\mathbf{x}+\mathbf{e}_5$, other neighbours are filled or interface cells. Therefore, the distribution functions $f_4'(\mathbf{x}, t+\Delta t)$ and $f_7'(\mathbf{x}, t+\Delta t)$ at position $\mathbf{x}$ and time $t+\Delta t$ have to be reconstructed according to Equation (9):

$$\begin{aligned} f_4'(\mathbf{x}, t+\Delta t) &= f_4^{\mathrm{eq}}(\rho(\mathbf{x}, t), \mathbf{u}(\mathbf{x}, t)) + f_2^{\mathrm{eq}}(\rho(\mathbf{x}, t), \mathbf{u}(\mathbf{x}, t)) - f_2(\mathbf{x}, t) \\ f_7'(\mathbf{x}, t+\Delta t) &= f_5^{\mathrm{eq}}(\rho(\mathbf{x}, t), \mathbf{u}(\mathbf{x}, t)) + f_7^{\mathrm{eq}}(\rho(\mathbf{x}, t), \mathbf{u}(\mathbf{x}, t)) - f_5(\mathbf{x}, t) \end{aligned} \tag{10}$$

where $\rho(\mathbf{x}, t) = 1$. In addition, in order to balance the forces on each side of the interface, the distribution functions coming from the interface normal direction $\mathbf{n}$ (i.e. when $\mathbf{n} \cdot \mathbf{e}_i < 0$) are also reconstructed using Equation (9). The interface normal direction $\mathbf{n}$ is calculated with the following central difference approximation:

$$\mathbf{n} = \sum_{i=1}^{8} s_i \mathbf{e}_i \varepsilon(\mathbf{x} + \mathbf{e}_i) \tag{11}$$

where $\mathbf{s} = \frac{1}{4}[2, 2, 2, 2, 1, 1, 1, 1]$ for D2Q9 BGK model.

2.2.3. Cell type re-initialization. All distribution functions for the interface cells are valid after reconstruction, and the standard collision can be performed. The density obtained from the collision step is now used to check whether the interface cell is new filled or new emptied during this time step. The criteria are:

$$\begin{aligned} m(\mathbf{x}, t+\Delta t) &> (1+\kappa)\rho(\mathbf{x}, t+\Delta t) \rightarrow \text{new filled cells} \\ m(\mathbf{x}, t+\Delta t) &< -\kappa\rho(\mathbf{x}, t+\Delta t) \rightarrow \text{new emptied cells} \end{aligned} \tag{12}$$

DOI: 10.1002/fld

Here, an addition offset $\kappa = 10^{-3}$ is used instead of 0 or 1 for the empty or filling thresholds to prevent the new surrounding interface cells from being reconverted in the following step. The positions of the new emptied or filled cells are stored in a list instead of immediately converting their types. The conversion will be done only when the main loop over all cells is completed.

The re-initialization step mainly takes place to new filled, new emptied cells and their neighbours. First, for the new filled cells, all neighbouring empty cells are converted to interface cells. For each of these cells, the average density ρ^{avg} and velocity $\mathbf{u}^{\text{avg}}$ of the surrounding fluid and interface cells are computed and the distribution functions of the empty cells are initialized with the equilibrium distribution $f_i^{\text{eq}}(\rho^{\text{avg}}, \mathbf{u}^{\text{avg}})$. The flags of the new filled cells are changed into fluid or filled. Likewise, for the new emptied cells, the surrounding cells are converted to interface cells, simply taking the former fluid cell's distribution functions for each corresponding new interface cell. Secondly, the excess mass m^{ex} is distributed among the surrounding interface cells through the following formula:

$$\begin{aligned} m^{\text{ex}} &= m - \rho \quad \text{for new filled cells} \\ m^{\text{ex}} &= m \qquad\quad \text{for new emptied cells} \end{aligned} \tag{13}$$

Negative mass values or mass values larger than the density mean that the fluid interface moves beyond the current cell during the last time step. The excess mass is weighted according to the interface normal direction $\mathbf{n}$, instead of being evenly distributed among the surrounding interface cells. The mass of the surrounding interface cells changes by

$$m(\mathbf{x} + \mathbf{e}_i, t + \Delta t) = m(\mathbf{x} + \mathbf{e}_i, t + \Delta t) + m^{\text{ex}} \cdot \frac{v_i}{v_{\text{total}}} \tag{14}$$

where

$$v_i = \begin{cases} \mathbf{n} \cdot \mathbf{e}_i \\ \qquad \text{if } \mathbf{n} \cdot \mathbf{e}_i > 0 \quad \text{for new filled cells} \\ 0 \end{cases}$$

$$v_i = \begin{cases} -\mathbf{n} \cdot \mathbf{e}_i \\ \qquad \text{if } \mathbf{n} \cdot \mathbf{e}_i < 0 \quad \text{for new emptied cells} \\ 0 \end{cases} \tag{15}$$

$$v_{\text{total}} = \sum_{i=0}^{8} v_i$$

Once the re-initialization is completed, the process can move on to the next time step.

2.3. Wall boundary conditions

For free surface problems, the wall boundaries can be decomposed into the walls in contact with the free surface and the walls which are submerged in the liquid fluid.

The fully submerged walls can be treated in a normal way by adhering to the no-slip boundary condition. A simple way to implement no-slip boundary conditions in the LBM is the bounce-back rule. In this method, all distribution functions are reflected at the boundary sites, back along the links they arrived on. Thus at a wall parallel to the direction of e_1 and e_3, as shown in Figure 3,

DOI: 10.1002/fld

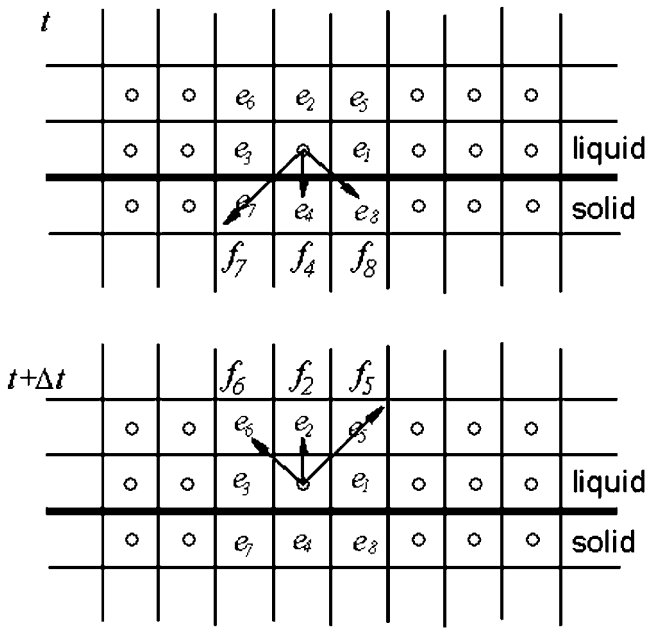

Figure 3. No-slip boundary conditions (bounce-back rules).

the distribution function approaching the boundary on links e_4, e_7 and e_8, will be bounced back along the links e_2, e_5 and e_6, respectively, resulting in $f_2 = f_4$, $f_5 = f_7$ and $f_6 = f_8$. Averaging the velocity at the boundary, before and after the collision step, gives the required no-slip boundary condition $\mathbf{u} = 0$.

The walls in contact with the free surface should be treated carefully, since the free surface is moving and the bounding wall is static. No introduction for treating this kind of boundaries can be found in the literature. In this paper, we develop a compound boundary condition for the free surface contacting solid wall as follows: Nothing needs to be done when the boundary cells are empty. Reconstruction is needed to complement those distribution functions streaming into the boundary cells from solid wall when the boundary cells are interface cells. This means that the boundary cells are treated as interface cells until they are filled. Once the boundary cells are filled, the bounce-back rule, i.e. no-slip boundary conditions will be applied. Among the wall boundary cells, as shown in Figure 4, those marked with 'F' stand for filled cells, no-slip boundary conditions as described above are applied to these cells. Those marked with 'E' stand for empty cells, thus nothing is needed to do. While those marked with 'I' stand for interface cells, all those distribution functions streamed from the wall cells into the interface boundary cells should be reconstructed according to Equation (9).

2.4. Gravity force

Buick [37] proposed several methods to incorporate external forces like gravity into the LBM. They are: (a) combining the gravity term with the pressure tensor when there is only a negligible

DOI: 10.1002/fld

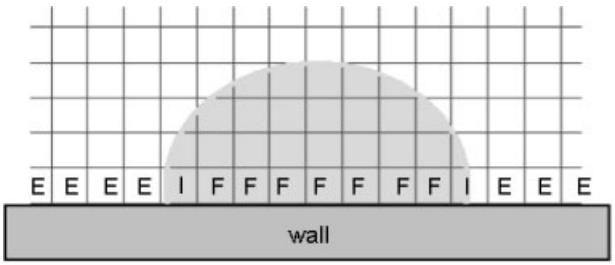

Figure 4. Boundary layer cells.

change in density ρ, (b) calculating the equilibrium distribution functions with an altered velocity, (c) adding an additional term to the collision function of the Boltzmann equation, and (d) a combination of the second and third methods. The second method is adopted in this paper and is given as below.

If a gravitational force $\mathbf{F}$ is applied, then at every time step there is a change of momentum which equals to $\mathbf{F}$. To incorporate this into the LBM model, the equilibrium distribution functions are expressed as

$$f_i^{\mathrm{eq}}(\mathbf{x}, t) = f_i^{\mathrm{eq}}(\rho, \mathbf{u}^*) \tag{16}$$

where $\mathbf{u}^*$ is given by

$$\rho\mathbf{u}^* = \rho\mathbf{u} + \tau\mathbf{F} \tag{17}$$

Details of this method can be found elsewhere [37, 52].

3. APPLICATIONS

To test the LBM-based single-phase method for free surface tracking, simulations are carried out for studying the motion of a free falling droplet with/without gravity and droplet spreading on a wall surface. Surface tension is not considered in this paper, and will be added in the future work. All the test cases are compared with the results obtained by using commercial CFD software Fluent with the VOF model. The VOF model treats all the cases mentioned above as the two-phase fluid systems and simulates the two-phase fluid motions by solving the Navier–Stokes equations and the convection equation for the volume ratio of the liquid phase. For VOF method, the interface tracking is achieved by estimating the normal vector of the interface, constructing the dividing planar surface (interface surface) in every computational grid, and propagation of the interface by the flow. In contrast to the standard VOF method, the single-phase method mainly consists of calculating the mass changes from the distribution function values of the LBM, reconstructing the unknown distribution functions streamed from empty cells into the interface cells, and propagating the interface by the flow (stream and collision steps of LBM). Details of VOF can be found in Reference [53].

DOI: 10.1002/fld

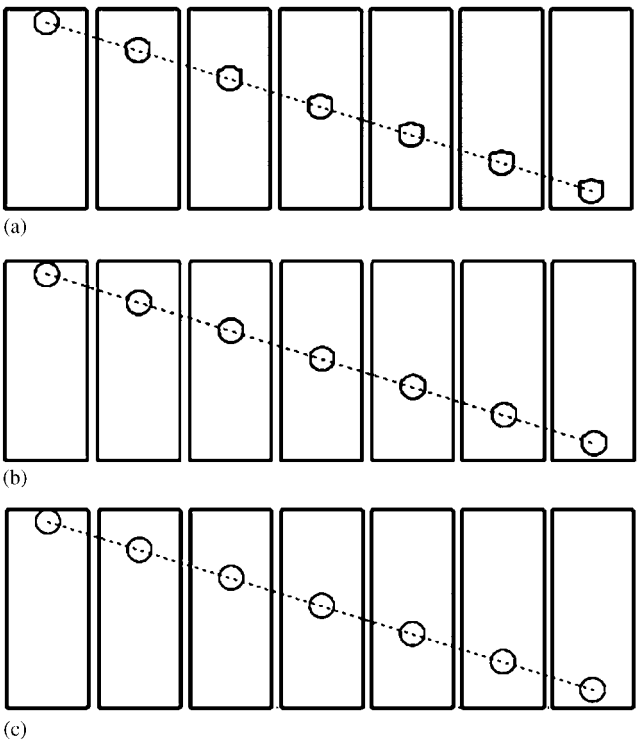

Figure 5. Grid size independent study with droplet falling down without gravity: (a) 100×250 lattices; (b) 200×500 lattices; and (c) 400×1000 lattices.

3.1. Falling droplet with/without gravity

2D free falling droplet motions are simulated in and without presence of the gravity. For case 1, gravity is not considered. The droplet falls with a constant velocity in stationary air. Reynolds number is chosen as $Re = 8.5$. For case 2, gravity is added. Initial velocity of the droplet is given as zero. The droplet falls down under the gravity effect.

Simulation of droplet falling without gravity are carried out with three difference lattices, 100×250, 200×500 and 400×1000 lattice units, respectively, to perform the grid independence study. The results are shown in Figure 5. It can be seen that the smaller the lattice size, the smoother the droplet shape, and thus the thinner the interface layer. The initial velocities are set as a constant. It can be seen that the falling velocities are kept very well with three different lattice sizes, which can be observed from the droplet positions at different times (with time intervals of 10^{-3} s) in Figure 5. The droplet falling distances increase linearly with time, suggesting a constant falling velocity. However, the computational cost is quite different. The smaller the lattice size, the higher the computational cost. The computational time using 400×1000 lattices is about 16 times long as that when using 200×500 lattices, and about 256 times long as that when using 100×250 lattices. However, the quality of the droplet shape is quite poor with 100×250 lattices. Therefore, based on the grid independence study, the simulations of droplet falling with/without gravity were

DOI: 10.1002/fld

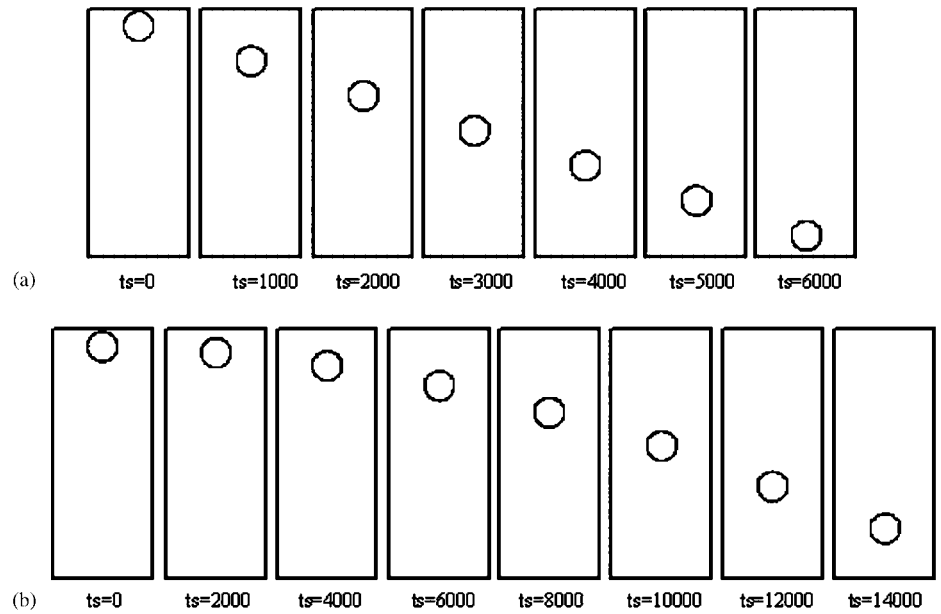

Figure 6. Results obtained from the LBM single-phase model: (a) droplet falling down without gravity; and (b) droplet falling down under the effect of gravity.

conducted with 200 lattices in horizontal direction and 500 lattices in vertical direction. With 200×500 lattices, the droplet shape is smooth and the computational cost is acceptable.

The test cases include a water/air system, i.e. droplet is water and is surrounded by air. For the LBM single-phase model, the kinematic viscosity of water is $v = 10^{-6}\,\mathrm{m}^2/\mathrm{s}$, grid scale $\Delta x = \sqrt{2} \times 10^{-6}\,\mathrm{m}$ and relaxation time $\tau = 2.0$. Since lattice viscosity $v^* = v \cdot (\Delta t/\Delta x^2)$, and it is related to the relaxation time τ through $v^* = (2\tau - 1)/6$, the lattice viscosity $v^* = 0.5$ and the time step size $\Delta t = 10^{-6}\,\mathrm{s}$. Lattice force of gravity is given by $g^* = g \cdot (\Delta t^2/\Delta x) = \frac{9.81}{\sqrt{2}} \times 10^{-6}$. These parameters are fixed for all test cases including droplet falling and the droplet spreading.

For droplet falling cases, no gas flow field boundaries need special treatment since the single-phase model only considers the fluid phase and ignores the gas phase. For the VOF model, the simulations are also implemented with 200 grid cells in horizontal direction and 500 in vertical direction. All the four boundaries are set as pressure outlet boundaries for both cases 1 and 2. Figures 6 and 7 show the time series of snapshots of a falling droplet obtained by the LBM single-phase model and the Fluent VOF model, respectively. Figures 6(a) and 7(a) display the results of case 1, while Figures 6(b) and 7(b) depict the results of case 2. The time interval corresponds to 1000 time steps, namely $10^{-3}\,\mathrm{s}$ for case 1 and 2000 time steps, namely $2.0 \times 10^{-3}\,\mathrm{s}$ for case 2. From Figures 6 and 7, it can be seen that the droplet motions obtained by the LBM single-phase model are quite similar to those from the Fluent VOF model, except that the shapes of the droplets differ. The droplet shape obtained from the LBM single-phase model is not very smooth and is deformed, which results from the absence of surface tension and relative coarse lattices chosen. Use of finer lattices as demonstrated in the grid independence study can definitely give a smoother

DOI: 10.1002/fld

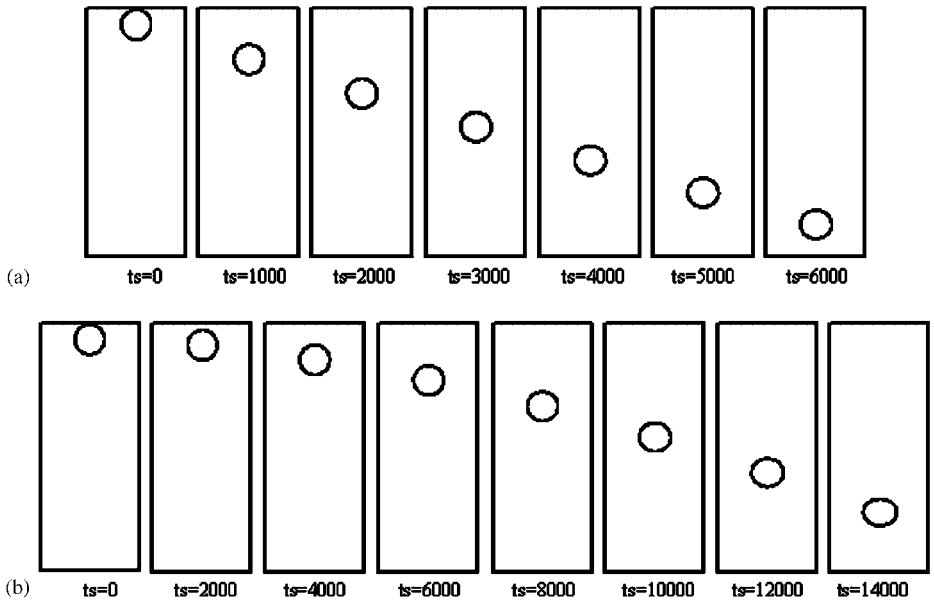

Figure 7. Results obtained from the Fluent VOF model: (a) droplet falling down without gravity; and (b) droplet falling down under the effect of gravity.

Table I. Errors and simulation efficiencies.

Model	Case	Velocity error	Mass error	Computational cost
Single-phase model	Case 1	3.75×10^{-16}	1.94×10^{-15}	6.53 hours/6000 time steps
	Case 2	1.76×10^{-8}	5.48×10^{-11}	10.38 hours/14 000 time steps
VOF model	Case 1	1.0×10^{-5}	1.0×10^{-5}	31.5 CPU hours/6000 time steps
	Case 2	1.0×10^{-5}	1.0×10^{-5}	73.5 CPU hours/14 000 time steps

interface shape, and incorporating surface tension would fix the deformation problem. Surface tension will be considered in our future studies.

In addition, the shape of the droplet obtained from the Fluent VOF model becomes flatter as it approaches to the bottom boundary. It is also due to the fact that surface tension is not included in the simulation. It is known that the presence of surface tension maintains the round shape of the droplet. Validation has been carried out using the Fluent VOF model by the authors.

Table I compares the computational errors of the velocity and mass conservation obtained by the single-phase model and the VOF model, as well as the computational cost of the two models. Velocity error is defined as

$$\text{velocity error} = \text{Max}\left[\frac{\sum_{\text{lattice or grid}} \text{simulated velocity at different time steps} - \sum_{\text{lattice or grid}} \text{theoretical value}}{\sum_{\text{lattice or grid}} \text{theoretical value}}\right] \tag{18}$$

DOI: 10.1002/fld

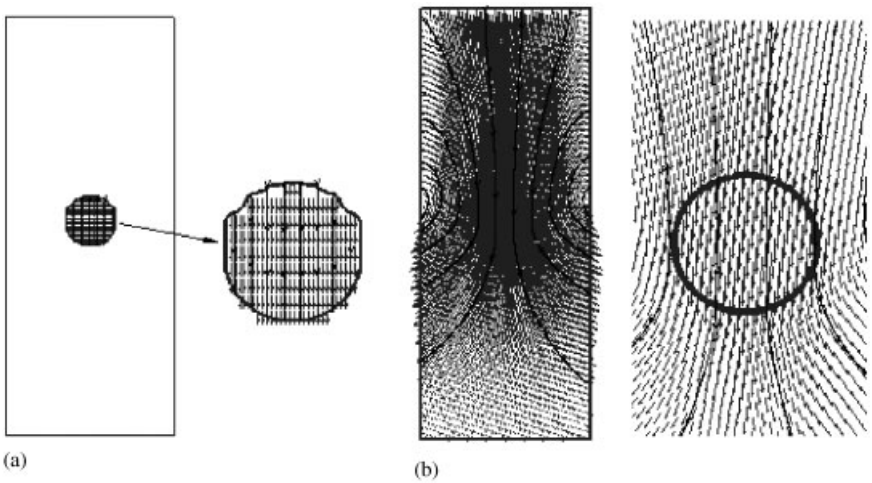

Figure 8. Velocity vectors and streamlines of case 1: (a) LBM single-phase model; and (b) Fluent VOF model.

While the mass conservation error is defined as

$$\text{mass error} = \text{Max}\left[\frac{\sum_{\text{lattice or grid}} \text{simulated mass at different time steps} - \sum_{\text{lattice or grid}} \text{initial mass}}{\sum_{\text{lattice or grid}} \text{initial mass}}\right] \tag{19}$$

For case 1, it only takes 6.53 CPU hours for 6000 time steps performed on Origin 3000 server for the LBM single-phase model. The velocity error is 3.75×10^{-16} and mass error is 1.94×10^{-15}. While it takes 31.5 CPU hours for 6000 time steps running on Origin 3000 server for the Fluent VOF model. For case 2, the time taken by the Fluent VOF model is about seven times longer than that by the LBM single-phase model. The lower computational efficiency of Fluent VOF model is due to the fact that it needs to solve the Navier–Stokes equations in the entire domain with 200×500 grid cells. Therefore, it can be concluded that the LBM single-phase model can simulate the free surface problem at high computational efficiency when the gas phase can be ignored.

Figures 8 and 9 compare the velocity vectors and streamlines obtained by the LBM single-phase model and the Fluent with VOF model for cases 1 and 2, respectively. Figure 8 shows the vectors and streamlines at 3000 time steps of case 1 and Figure 9 corresponds to the results at 12 000 time steps of case 2. As the single-phase model ignores the gas phase except that during the computation the gas pressure at the fluid interface is applied by reconstructing the missing information from the gas phase, no velocity field is shown in the gas phase. The Fluent VOF model however needs to solve the Navier–Stokes equations in the entire domain with 200×500 grid cells, and thus gives the flow field in terms of the velocity vectors and streamlines in both the liquid and gas phases. Nonetheless, it is clear that both methods give similar flow fields inside the droplet. Uniform flow fields are observed. This demonstrates that though ignorance of the gas phase effect, the LBM single-phase model is still able to simulate free surface problems with satisfactory accuracy and high efficiency.

DOI: 10.1002/fld

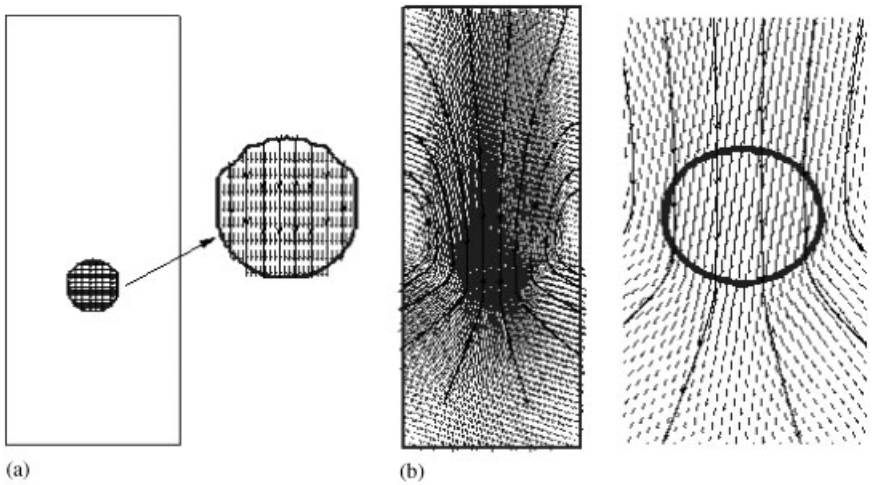

Figure 9. Velocity vectors and streamlines of case 2: (a) LBM single-phase model; and (b) Fluent VOF model.

3.2. Droplet spreading on a wall surface under gravity

Grid independence study was also carried out for the droplet spreading problem. The simulations show that use of 200×100 (horizontal $\times$ vertical) lattice units can produce grid independence results for droplet spreading on a wall surface under gravity. The initial velocity of the droplet is set as zero.

As for the substrate wall boundary conditions, the LBM single-phase model applies no-slip boundary conditions for the fully submerged wall boundary cells and uses the special treatment (as described in Section 2.3) for the wall boundary cells in contact with the free surface. In the Fluent VOF model, no-slip boundary conditions are applied on the substrate solid wall, and pressure outlet boundary conditions for the other boundaries. For simplicity, surface tension and wetting are not considered in both the models, but they will be considered in our further studies. Figures 10 and 11 show the simulation results for the time evolution of the droplet shapes as it spreads under gravity by the LBM single-phase model and the Fluent VOF model, respectively. It can be seen that the profiles of the droplet corresponding to different times obtained from the LBM single-phase model are virtually indistinguishable to those obtained from the Fluent VOF model. Figure 12 shows a comparison of the droplet spreading dynamics, in terms of the dimensionless height (defined as H/D_0 and displayed as solid lines) and the dimensionless width (defined as D/D_0 and displayed as dashed lines) versus time (where D_0 is the initial diameter of the droplet). Lines with filled square symbols are the results from the Fluent VOF model and lines with triangle symbols are from the LBM single-phase model. It is noted that there is good agreement between the LBM model and the Fluent VOF model.

From comparison, it can be seen that both the droplet profile and the spreading dynamics obtained from the single-phase model have very good agreement with those from the VOF model. It can be concluded that the LBM single-phase model is successfully implemented for the simulation of the free surface droplet spreading under gravity. It also can be noted that the interface layer obtained by the single-phase model is quite thin compared with those obtained by the VOF model

DOI: 10.1002/fld

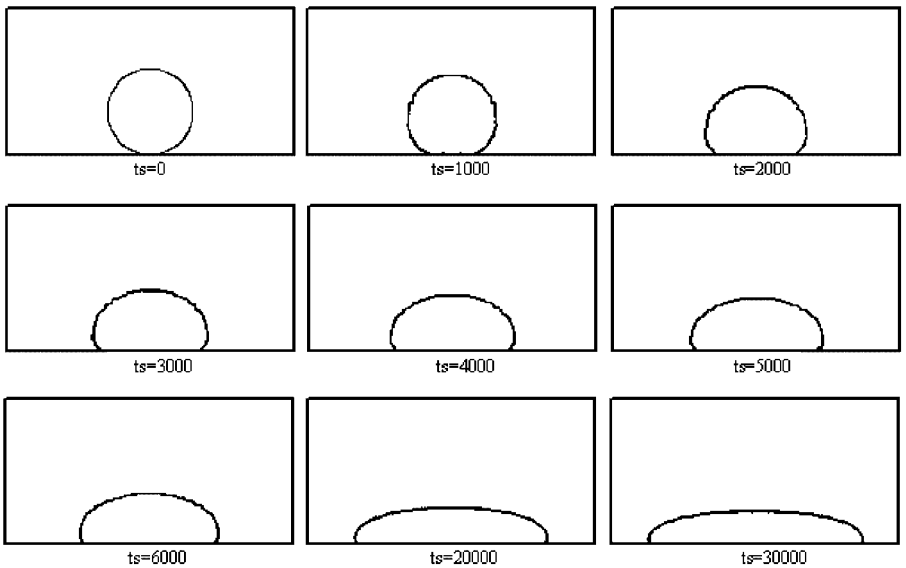

Figure 10. Results of droplet spreading obtained from the LBM single-phase model.

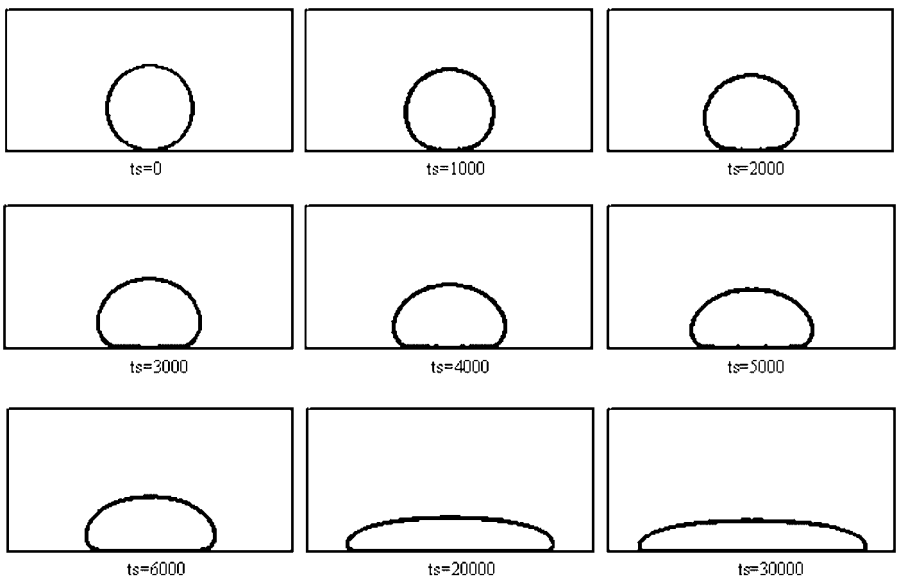

Figure 11. Results of droplet spreading obtained from the Fluent VOF model.

which can also be observed in the droplet falling cases. This is mainly because the interface cells form a closed layer between fluid and empty cells in the single-phase model and only one layer of interface cells form the interface layer.

DOI: 10.1002/fld

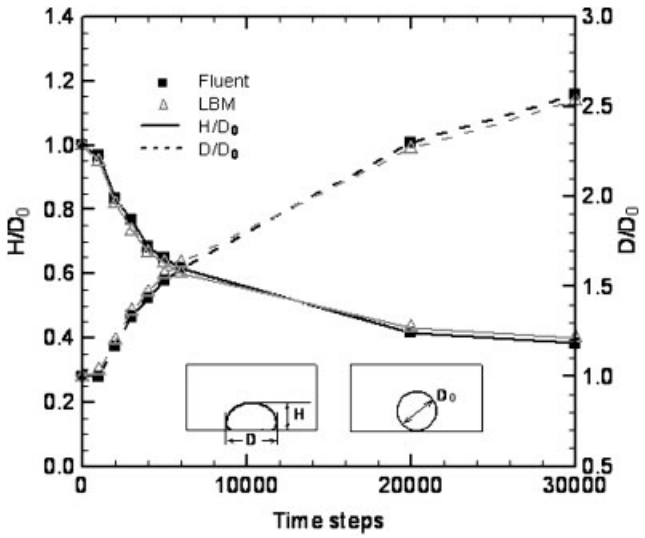

Figure 12. Comparison of spreading speed.

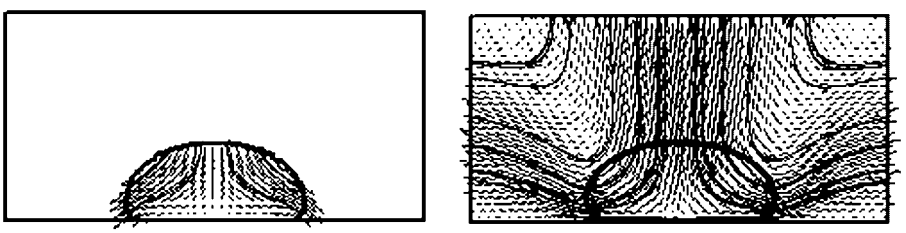

Figure 13. Velocity vectors and streamlines of droplet spreading: (a) LBM single-phase model; and (b) Fluent VOF model.

Figure 13 shows a comparison between the LBM single-phase model and the Fluent VOF model for the velocity vectors and streamlines. The symmetry of the velocity vectors and the streamlines in both the flow fields are very good, suggesting the success of the simulations. As for the computational cost, the VOF model needs to solve the Navier–Stokes equations to obtain the flow field in the entire computational domain with 200×100 grid cells, while the single-phase model only needs to handle the cells filled with fluid. Therefore, the computational cost of VOF model is much higher than that of the single-phase model.

4. CONCLUSIONS

A single-phase free surface tracking algorithm-based LBM method has been successfully developed and implemented to simulate the motions of a falling droplet with and without gravity and droplet spreading on a solid surface under gravity.

DOI: 10.1002/fld

The LBM single-phase method simulations have been compared with the results obtained from the commercial CFD software Fluent. The former ignores the gas phase; the latter treats the free surface problem in our test cases as two-phase systems and uses VOF model to track the fluid surface. It is found that the simulations with the LBM single-phase model are in good agreement with those from the VOF model, suggesting that the LBM single-phase model is able to simulate free surface problems with/without considering the gravity. The simulation results show that the boundary conditions for the walls in contact with the free surface proposed in this study are reasonable and can give satisfactory simulation results of droplet spreading on a wall surface under gravity effect. Comparison also suggests the LBM single-phase model has an obvious higher computational efficiency.

ACKNOWLEDGEMENTS

The authors thank the Agency for Science, Technology and Research for supporting this research through Project Number 0421010018.

REFERENCES

1. He X, Chen S, Zhang R. A lattice Boltzmann scheme for incompressible multiphase flow and its application in simulation of Rayleigh–Taylor instability. *Journal of Computational Physics* 1999; **152**:642–663.
2. Dellar PJ. Lattice and discrete Boltzmann equations for fully compressible flow. *Proceeding of 3rd MIT Conference on Computational Fluid and Solid Mechanics*, MIT, 2005.
3. Chen S, Dawson SP, Doolen GD, Janecky DR, Lawniczak A. Lattice methods and their application to reacting systems. *Computers and Chemical Engineering* 1995; **19**:617–646.
4. Verberg R, Ladd AJC. Simulation of chemical erosion in rough fractures. *Physical Review E* 2002; **65**:056311.1-6.
5. Yu H, Luo S, Girimaji SS. Scalar mixing and chemical reaction simulations using lattice Boltzmann method. *International Journal of Computational Engineering Science* 2001; **3**:73–87.
6. Ladd AJC. Numerical simulations of particulate suspensions via a discretized Boltzmann equation. Part 1. Theoretical foundation. *Journal of Fluid Mechanics* 1994; **271**:285–309.
7. Ladd AJC. Numerical simulations of particulate suspensions via a discretized Boltzmann equation. Part 2. Numerical results. *Journal of Fluid Mechanics* 1994; **271**:311–339.
8. Ladd AJC. Short-term motion of colloidal particles: numerical simulations via a fluctuating Lattice–Boltzmann equation. *Physical Review Letters* 1993; **70**:1339–1342.
9. Ladd AJC, Verberg R. Lattice Boltzmann simulations of particle-fluid suspensions. *Journal of Statistical Physics* 2001; **104**:1191–1251.
10. Behrand O. Solid–fluid boundaries in particle suspension simulations via the lattice Boltzmann method. *Physical Review E* 1995; **52**:1164–1175.
11. Aidun CK, Lu Y-N. Lattice Boltzmann simulation of solid particles suspended in a fluid. *Journal of Statistical Physics* 1995; **81**:49–61.
12. Masselot A, Chopard B. A lattice Boltzmann model for particle transport and deposition. *Europhysics Letters* 1998; **42**:259–264.
13. Hagen MHJ, Frenkel D, Lowe CP. Rotational diffusion in dense suspensions. *Physica A* 1999; **272**:376–391.
14. Hagen MHJ, Pagonabarraga I, Lowe CP, Frenkel D. Algebraic decay of velocity fluctuations in a confined fluid. *Physical Review Letters* 1997; **78**:3785–3788.
15. Lowe CP, Frenkel D, Masters AJ. Long-time tails in angular momentum correlations. *Journal of Chemical Physics* 1995; **103**:1582–1587.
16. Heemels MW, Hagen MHJ, Lowe CP. Simulation of solid colloidal particles using the Lattice–Boltzmann method. *Journal of Computational Physics* 2000; **164**:48–61.
17. Koponen A, Kandhai D, Hellen E, Alava M, Hoekstra A, Kataja M, Niskanen K, Sloot P, Timonen J. Permeability of three-dimensional random fiber webs. *Physical Review Letters* 1998; **80**:716–719.
18. Lowe CP, Frenkel D. Do hydrodynamic dispersion coefficients exist?. *Physical Review Letters* 1996; **77**:4552–4555.

DOI: 10.1002/fld

19. Koch DL, Hill RJ, Sangani AS. Brinkman screening and the covariance of the fluid velocity in fixed beds. *Physics of Fluids* 1998; **10**:3035–3037.
20. Ahlrichs P, Dünweg B. Simulation of a single polymer chain in solution by combining lattice Boltzmann and molecular dynamics. *Journal of Chemical Physics* 1999; **111**:8225–8239.
21. Guo Z, Zhao TS, Shi Y. A lattice Boltzmann algorithm for electro-osmotic flows in microfluidic devices. *Journal of Chemical Physics* 2005; **122**:144907.1-10.
22. Guo Z, Zhao TS, Shi Y. A lattice Boltzmann model for convection heat transfer in porous media. *Numerical Heat Transfer*, *Part B* 2005; **47**:157–177.
23. He X, Chen S, Doolen GD. A novel thermal model for the lattice Boltzmann method in incompressible limit. *Journal of Computational Physics* 1998; **146**:282–300.
24. Inamuro T, Yoshino M, Inoue H, Mizuno R, Ogino F. A lattice Boltzmann method for a binary miscible fluid mixture and its application to a heat-transfer problem. *Journal of Computational Physics* 2002; **179**:201–215.
25. Shan X. Simulation of Rayleigh–Benard convection using a lattice Boltzmann method. *Physical Review E* 1997; **55**:2780–2788.
26. Gunstensen AK, Rothman DH. Lattice Boltzmann model of immiscible fluids. *Physical Review A* 1991; **43**:4320–4327.
27. Rothman DH, Keller JM. Immiscible cellular-automation fluids. *Journal of Statistical Physics* 1988; **52**:1119–1127.
28. Grunau D, Chen S, Eggert K. A lattice Boltzmann model for multiphase fluid flows. *Physics of Fluids*, *Part A* 1993; **5**:2557–2562.
29. D'Ortona U, Salin D, Cieplak M, Rybka RB, Banavar JR. Two-color nonlinear Boltzmann cellular automata: surface tension and wetting. *Physical Review E* 1995; **51**:3718–3728.
30. Nie X, Qian Y, Doolen GD, Chen S. Lattice Boltzmann simulation of the two-dimensional Rayleigh–Taylor instability. *Physical Review E* 1998; **58**:6861–6864.
31. Shan X, Chen H. Lattice Boltzmann model for simulating flows with multiple phases and components. *Physical Review E* 1993; **47**:1815–1819.
32. Shan X, Chen H. Simulation of non-ideal gases and liquid–gas phase transitions by the lattice Boltzmann equation. *Physical Review E* 1994; **49**:2941–2948.
33. Shan X, Doolen GD. Multicomponent lattice Boltzmann model with interparticle interaction. *Journal of Statistical Physics* 1995; **81**:379–393.
34. Orlandini E, Swift MR, Yeomans JM. Lattice Boltzmann model of binary-fluid mixtures. *Europhysics Letters* 1995; **32**(6):463–468.
35. Swift MR, Osborn WR, Yeomans JM. Lattice Boltzmann simulation of nonideal fluids. *Physical Review Letters* 1995; **75**(5):830–834.
36. Swift MR, Orlandini E, Osborn WR, Yeomans JM. Lattice Boltzmann simulations of liquid–gas and binary fluid systems. *Physical Review E* 1996; **54**:5041–5052.
37. Buick JM. Lattice Boltzmann methods in interfacial wave modeling. *Ph.D. Thesis*, University of Edinburgh, U.K., 1997.
38. Buick JM, Cosgrove JA, Greated CA. Gravity-capillary internal wave simulation using a binary fluid lattice Boltzmann model. *Applied Mathematical Modeling* 2004; **28**:183–195.
39. Xu A, Gonnella G, Lamura A. Phase-separating binary fluids under oscillatory shear. *Physical Review E* 2003; **67**:0561052-14.
40. Dupuis A, Yeomans JM. Modelling droplets on superhydrophobic surfaces: equilibrium states and transitions. *Langmuir* 2005; **21**:2624–2629.
41. Dupuis A, Yeomans JM. Lattice Boltzmann modelling of droplets on chemical heterogeneous surfaces. *Future Generation Computer System* 2004; **20**:993–1001.
42. Palmer BJ, Rector DR. Lattice Boltzmann algorithm for simulating thermal two-phase flow. *Physical Review E* 2000; **61**:5295–5306.
43. Takada N, Misawa M, Tomiyama A, Hosokawa S. Simulation of bubble motion under gravity by lattice Boltzmann method. *Journal of Nuclear Science and Technology* 2001; **38**(5):330–341.
44. Zhang JM, Mohammadi R, Kwok DY. Droplet movements and continuous flows in rough and hydrophobic microchannels. *Proceeding of ICMM2005*, *3rd International Conference on Microchannels and Minichannels*, Toronto, Ontario, Canada, 13–15 June 2005.
45. Chang Q, Alexander JID. Numerical analysis of spreading of liquid droplet on a heterogeneous surface by the lattice Boltzmann method. ICMM2005-75139, *Proceeding of ICMM2005*, *3rd International Conference on Microchannels and Minichannels*, Toronto, Canada, 13–15 June 2005.

DOI: 10.1002/fld

46. Ginzburg I, Steiner K. Lattice Boltzmann model for free surface flow and its application to filling process in casting. *Journal of Computational Physics* 2003; **185**:61–99.
47. Thürey N. A single-phase free surface lattice Boltzmann method. *Masters Thesis*, University of Erlangen, Nuremberg, Germany, 2003.
48. Thürey N, Rüde U. Free surface Lattice Boltzmann fluid simulations with and without level sets. *Workshop on Vision*, *Modelling and Visualization*, vol. 2. IOS Press: Standford, CA, U.S.A., 2004; 199–208.
49. Thürey N, Rüde U, Körner C. Interactive free surface fluids with the lattice Boltzmann method. *Technical Report*, University of Erlangen, Nuremberg, Germany, 2005.
50. Körner C, Pohl T, Rüde U, Thürey N, Zeiser T. Parallel lattice Boltzmann methods for CFD applications. In *Numerical Solution of Partial Differential Equations on Parallel Computers*, Bruaset AM, Tveito A (eds). Springer: Berlin, 2005; 439–465.
51. Qian YH, D'Humieres D, Lallemand P. Lattice BGK models for Navier–Stokes equation. *Europhysics Letters* 1992; **17**:479–484.
52. Buick JM, Greated CA. Gravity in a lattice Boltzmann model. *Physical Review E* 2000; **61**:5307–5320.
53. Hirt CW, Nichols BD. Volume of fluid (VOF) method for the dynamics of free boundaries. *Journal of Computational Physics* 1981; **39**:201–225.

DOI: 10.1002/fld